# Diffusion and synchronization in an ion-trap resonator

H. B. Pedersen, D. Strasser, B. Amarant, O. Heber, M. L. Rappaport, and D. Zajfman*
*Department of Particle Physics, Weizmann Institute of Science, Rehovot, 76100, Israel*
(Received 23 October 2001; published 18 March 2002)

The motion of an ion bunch trapped between two electrostatic mirrors in an ion-trap resonator is analyzed both experimentally and via numerical simulations. It is found that under certain conditions it is possible to achieve either synchronization of the ion motion, which causes the size of the bunch to remain constant, or enhanced diffusion, which leads to rapid debunching. These effects are analyzed and criteria for synchronization are proposed.

DOI: 10.1103/PhysRevA.65.042704 PACS number(s): 34.80.Gs

## I. INTRODUCTION

Ion traps are able to trap charged particles for a long time, and they have been successfully applied in several areas of physics [1]. Among the many applications of ion traps is their use for atomic and molecular physics, such as for the study of metastable states [2], and cluster cooling [3]. The dynamics of trapped ions has drawn much attention since the early days of ion trapping [4–7]. One item of interest in these systems stems from collective effects which can be studied both in the laboratory under well defined conditions and with developed theoretical methods.

Recently, a different class of ion traps has been developed [8–12], in which ions oscillate between a pair of electrostatic mirrors, much like photons in an optical resonator. The trapped ions have kinetic energies of a few keV in the central part of the trap while inside the mirrors they have only a few meV near their turning points, where they are also subject to radial focusing forces. Thus, the density of ions changes strongly within the trap, due both to their slowing down inside the mirrors and to the radial focusing. This density can increase by two to three orders of magnitude inside the mirrors as compared to its value in the field-free region of the trap.

In a previous publication [13], we have investigated the stability criteria and ion loss mechanisms for ion beams stored in such a trap. Two regions of stability were experimentally identified, and these were found by both numerical simulation and optical models to be distinct modes with very different dynamical properties. Recently, we have also demonstrated [14] that the trapped ions can synchronize their motion under certain conditions. This effect was identified by observing that the size of a packet of ions remained constant for a practically unlimited time, i.e., the debunching that is usually observed did not occur. The synchronization effect was attributed to the repulsive Coulomb interaction between the ions [14].

In this paper, we provide experimental evidence for the dynamics of both diffusion and synchronization in our electrostatic trap by experimentally investigating a particular set of trap configurations. We numerically study two one-dimensional model systems, which illustrate the dynamics of diffusion and synchronization. Finally, we describe in more detail the dynamical basis of diffusion and synchronization and compare the results to numerical trajectory calculations. We find that the repulsive Coulomb interaction between the ions, in combination with the kinematical properties dictated by the electrostatic fields, can either enhance the diffusion, and hence speed up the transition to a steady state beam, or induce so strong a correlation between the ions that ion motion synchronization and self-ordering phenomena emerge.

## II. EXPERIMENTAL SETUP

### A. The ion trap

Experiments were performed with ion beams of $Ar^+$ and $Xe^+$. The ions were produced in an electron impact ion source, extracted, and accelerated to an energy of 4.2 keV. The ions were then mass analyzed by a 20° magnet positioned just after the ion source and by a 45° magnet positioned about 5 m from the ion source. Steering and focusing of the ions between the two magnets and between the last magnet and the ion trap were done with the help of two electrostatic quadrupole triplets. The ion currents measured with a Faraday cup located after the trap were $\sim 300$ nA for $Ar^+$ and $\sim 100$ nA for $Xe^+$. Ion bunches of 0.2–100 $\mu$s were created with an electrostatic chopper located before the first magnet. Shorter bunches ($<0.2$ $\mu$s) were created by rapidly sweeping one of the potentials of the quadrupole triplet through the value that allowed transmission of the beam to the trap.

A schematic drawing of the electrostatic ion trap is shown in Fig. 1. The mechanical design of the ion trap and its operation have been described previously [8,9]. Briefly, the ion trap consists of two coaxial electrostatic mirrors each composed of a stack of eight cylindrical electrodes. The configuration of the trap is characterized by the potentials on five of these electrodes, $V_1, V_2, V_3, V_4, V_z$ (see Fig. 1), the other three being grounded. Provided that the field generated by these potentials fulfills certain criteria, ions can be trapped oscillating between the two mirrors [8,9,13,15]. The ion trap is pumped by a cryopump to a pressure of $\sim 5 \times 10^{-10}$ Torr.

Injection of an ion bunch into the trap is performed by grounding all the entrance electrodes. The electrodes on the

*Author to whom correspondence should be addressed. FAX: +972-8-9344166. Email address: fndaniel@wicc.weizmann.ac.il

 

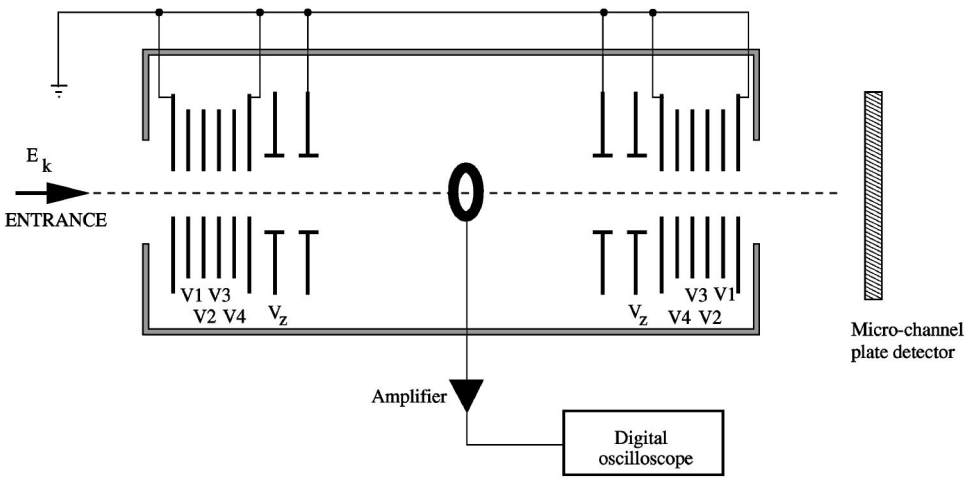


FIG. 1. Schematic view of the ion beam trap. The bunch is injected through the left side of the trap. The central ring represents the pick-up electrode. The microchannel plate (MCP) is $\sim 500$ mm to the right of the exit mirror.

other side are kept at high potential so that the bunch is reflected toward the entrance. Before the ion bunch returns to the entrance mirror, the potentials of its electrode are rapidly ($\sim 100$–$200$ ns) raised and the ion bunch is thus confined between the mirrors. The typical lifetime of the beam is $\sim 2$–$5$ s. In this paper, a particular set of trap configurations is investigated, namely, $\{V_1, V_2, V_3, V_4, V_z\} = \{V_1, 4.875 \text{ kV}, 3.25 \text{ kV}, 1.625 \text{ kV}, 4.06 \text{ kV}\}$, where $4.0 < V_1 < 6.5$ kV. This configuration is characterized by a high value of $V_z$, which causes the ions to be strongly focused inside the mirror region for all values of $V_1$ [13].

### B. Detection of trapped ions

The evolution of ion bunches during storage was monitored with a cylindrical pickup electrode made with a length $l_p = 7$ mm and inner diameter of 18 mm located at the center of the trap (see Fig. 1). The total capacitance of the pickup electrode plus leads was measured to be $C_p \sim 10$ pF. The pickup electrode was connected to the gate of a junction field effect transistor (JFET) whose drain was fed to a charge sensitive amplifier with feedback capacitance $C_f$. The amplified signal was recorded with a digital oscilloscope at a sampling rate of 12 MHz.

The charge induced on the pickup (in SI units) due to a single ion $j$ is given by

$$q_j(t) = \varepsilon_0 \int \mathbf{E}_j(\mathbf{r}_j, t) \cdot \mathbf{dS}, \tag{1}$$

where $\varepsilon_0$ is the vacuum permittivity, $\mathbf{E}_j(\mathbf{r}_j, t)$ is the electric field induced by the ion at position $\mathbf{r}_j$ at time $t$, and the integral is performed over the surface of the pickup. The corresponding potential present on the gate of the JFET is $V_j(t) = q_j(t)/C_p$. The signal $V_A$ measured by the oscilloscope is given by

$$V_A(t) = \frac{1}{C_f} \sum_j q_j(t) = \frac{Q_p(t)}{C_f}, \tag{2}$$

where the summation is over all the ions stored in the trap, and $Q_p(t)$ is the total induced charge at time $t$. The detection system was calibrated by injection of a known charge through a test capacitor of 1 pF using a potential step generator with a fast rise time ($<20$ ns). The calibration agrees with Eq. (2) using $C_f = 1.3$ pF.

The area $A$ under the pulse measured on the oscilloscope is proportional to the number of ions in a bunch $N$ and is given by

$$A = \frac{qN}{C_f} \frac{l_p}{v}, \tag{3}$$

where $v$ and $q$ are the ion velocity and charge, respectively. For a 4.2 keV bunch of $Ar^+$, $A(\mu\text{s mV}) = 7 \times 10^{-6} N$. Figure 2(a) shows a typical signal measured for $Ar^+$, 200 $\mu$s after injection. The peaks correspond to the passage of about $10^6$ ions through the pickup, and this signal is negative due to the polarity of the amplifier. As the actual bunch width is always larger than the length of the pickup electrode $l_p$, the measured width of the signal $W_n$ [see Fig. 2(a)] is a direct measurement of the bunch length itself. For a 4.2 keV $Ar^+$ beam, the electrode length is equal to a bunch length of $2W = 50$ ns.

### C. Detection of ion loss

The loss of ions from the trap is due to three processes: ion-ion scattering, ion-neutral scattering, and charge exchange (with the residual gas). Among these three, only the last leads to the production of neutral particles which exit the trap. These neutrals are detected using a microchannel plate, located $\sim 500$ mm after the trap, as shown in Fig. 1. The MCP signal is proportional to the number of ions stored in the trap, as described in Ref. [13]. Figure 3 shows typical decay curves measured with the MCP for two trap configurations.

## III. BUNCH DYNAMICS

The dynamics of a trapped ion bunch can be observed in the evolution of its size. The longitudinal diffusive motion of the ions in a bunch derives from four mechanisms. First, the ions will dephase due to the intrinsic spread of oscillation times $\Delta T_i$ which exists because the trapped ions move on trajectories with slightly different oscillation times. $\Delta T_i$ is characteristic of the trap configuration and the injection con-

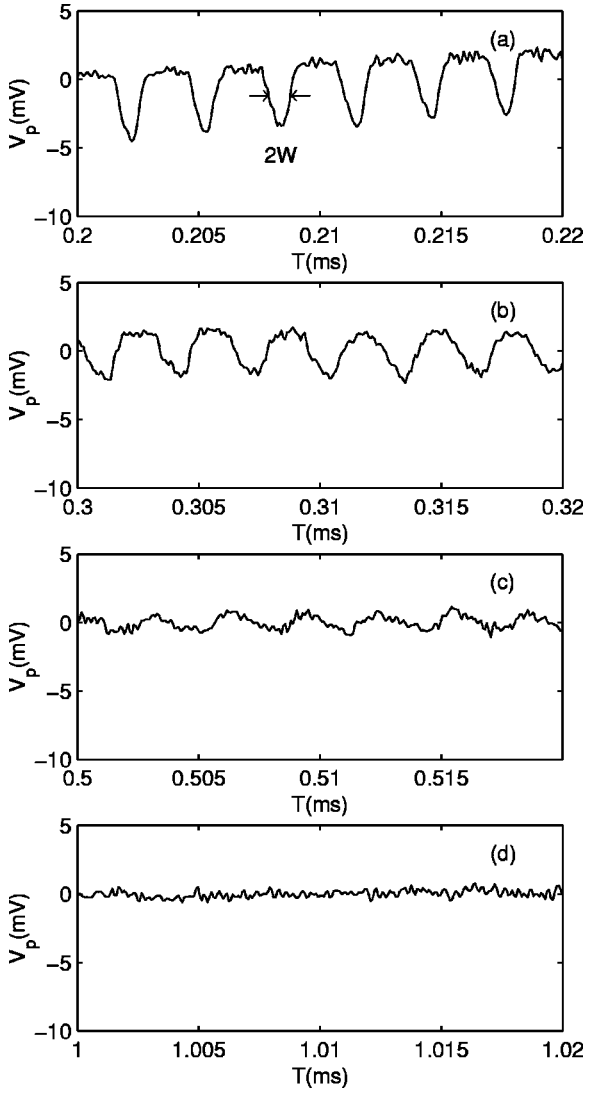


FIG. 2. Signal observed with the pickup for a 4.2 keV $Ar^+$ bunch with an initial width 170 ns stored with $V_1=5.5$ kV, at four different time intervals after injection: (a) 0.2–0.22 ms, (b) 0.3–0.32 ms, (c) 0.5–0.52 ms, and (d) 1.0–1.02 ms.

ditions. Second, the ions have an initial energy spread $\Delta E_0$ as they emerge from the ion source, giving rise to an additional width of oscillation times $\Delta T_v$. The exact dependency of oscillation time on ion energy is a function of the particular ion trajectory, and hence this time spread depends on both the applied trap configuration and the injection conditions. Third, the trapped ions are subject to *external* perturbations due to scattering on the residual gas and noise on the applied electrode potentials. Finally, the Coulomb repulsion between the ions leads to an *internal* perturbation of their motion and hence affects the diffusion pattern.

To evaluate the diffusion dynamics explicitly, we consider an ion bunch of temporal width $W_0$ initially positioned at the center of the trap. The time of arrival of ion $i$ at the center of the trap after $n$ oscillations is written as

$$t_n'(i)=t_s(i)+t_n(i) \tag{4}$$

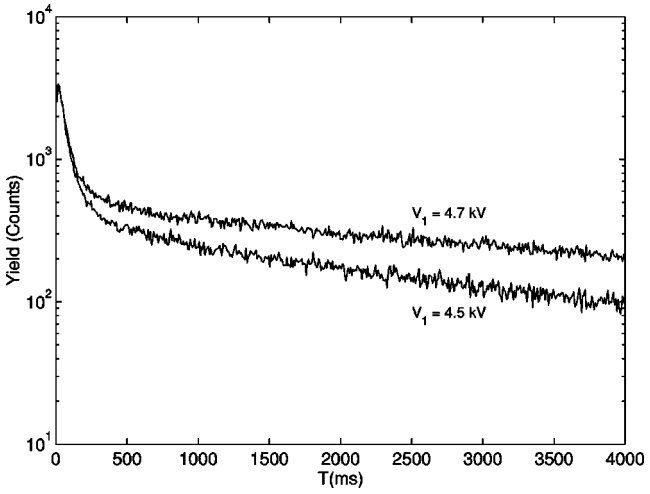


FIG. 3. Decay curves of trapped 4.2 keV $Ar^+$. The curves show the rates of $Ar^0$ atoms measured by the MCP detector and averaged over 200 injections, for two different configurations of the trap: $V_1=4.7$ kV (upper curve) and $V_1=4.5$ kV (lower curve).

where $t_s(i)$ is the initial time and $t_n(i)$ is explicitly given by

$$t_n(i)=\sum_{j=1}^{n} T_j(i) \tag{5}$$

where $T_j(i)$ is the oscillation time of ion $i$ during oscillation number $j$. Since the initial width ($W_0$) of the ion bunch is independent of the diffusion process, the bunch width $W_n$ after $n$ oscillations is given by

$$W_n=\sqrt{W_0^2+\langle t_n^2\rangle-\langle t_n\rangle^2}=\sqrt{W_0^2+\Delta t_n^2}, \tag{6}$$

where the averages are performed over the trapped ions. The distribution of oscillation times in oscillation $n$ is characterized by a mean $\langle T_n\rangle$ and a width $\Delta T_n$. The width of the distribution of arrival times at the center of the trap can now be written as

$$\Delta t_n^2=\Delta t_{n-1}^2+\Delta T_n^2+2\langle(T_n-\langle T_n\rangle)(t_{n-1}-\langle t_{n-1}\rangle)\rangle. \tag{7}$$

It is evident that, with $\Delta t_0=0$, Eqs. (6) and (7) allow the iterative evaluation of the width of the bunch after any number of oscillations. In the following we consider some implementations of Eqs. (6) and (7).

With neither external nor internal perturbations, the ions are characterized by a distribution of oscillation times with constant mean $\langle T_n\rangle=T$ and width $\Delta T_n=\Delta T_p$ given by

$$\Delta T_p=\sqrt{\Delta T_v^2+\Delta T_i^2}. \tag{8}$$

Hence the trapped ions behave as if they were a closed system where each ion preserves its initial oscillation time. In this case Eq. (7) reduces to

$$\Delta t_n^2=\Delta t_{n-1}^2+(2n-1)\Delta T_p^2=n^2\Delta T_p^2 \tag{9}$$

and the bunch width becomes

$$W_n = \sqrt{W_0^2 + n^2 \Delta T_p^2} \quad \text{(coherent diffusion)}. \tag{10}$$

We label this type of diffusion ''coherent diffusion,'' since the phase of each ion oscillator evolves unperturbed from its initial value.

On the other hand, if we assume that the ions interact with external perturbations so that the oscillation time of each ion is changed stochastically after each oscillation according to the distribution of oscillation times possible for the specific trap configuration ($\Delta T_p$), the last term in Eq. (7) vanishes, and $\Delta t_n^2 = \Delta t_{n-1}^2 + \Delta T_p^2 = n \Delta T_p^2$, which in turn leads to

$$W_n = \sqrt{W_0^2 + n \Delta T_p^2} \quad \text{(non-coherent diffusion)}. \tag{11}$$

Under these conditions, the bunch expands in a noncoherent way, i.e., the phase of each ion oscillator evolves stochastically. This form reflects the central limit theorem of statistical mechanics [16].

The expression for noncoherent diffusion, Eq. (11), relies explicitly on the randomization of oscillation times after *each* oscillation. A more general result describing the effect of stochastic interactions on the diffusion pattern is obtained by defining a number $n_{mix}$ equal to the average number of oscillations before an ion's oscillation time is randomized, i.e., the probability for an ion to change its oscillation time per oscillation is $1/n_{mix}$. Within this model Eq. (7) becomes

$$\Delta t_n^2 = \Delta t_{n-1}^2 + \Delta T_p^2 + 2 \Delta T_p^2 (n-1) \exp(-n/n_{mix}). \tag{12}$$

Equation (12) represents the general situation between the coherent and noncoherent diffusion: for $n_{mix} \to \infty$ Eq. (10) is recovered, while $n_{mix} \to 0$ gives Eq. (11). In any case, Eq. (12) shows that with purely stochastic perturbations of the ion motion the diffusion pattern is bounded between the two limiting cases Eq. (10) and Eq. (11).

Finally, if the ion motion is subject to internal perturbations from ion-ion collisions the value of $\Delta t_n$ [Eq. (7)] is a function of the trap configuration, the ion density, and the exact nature of the interaction. It is the object of this paper to look at the effect of this ion-ion interaction on the diffusion pattern in more detail.

## IV. EXPERIMENTAL RESULTS

### A. Diffusion

Figure 2 illustrates the evolution of a bunch of 4.2 keV $Ar^+$ ions, injected with an initial width of about 170 ns, as obtained for a trap configuration with $V_1 = 5.5$ kV. The figure shows the signal measured by the pickup for four time intervals after injection. The ion bunch is seen to broaden with time, becoming indistinguishable from the noise after about 1 ms.

The temporal evolution of the bunch was quantified by fitting each peak with a Gaussian profile on a linear background:

$$V(t) = -\frac{A}{\sqrt{2\pi} W_n} e^{-(t-t_b)^2/2W^2} + at + b \tag{13}$$

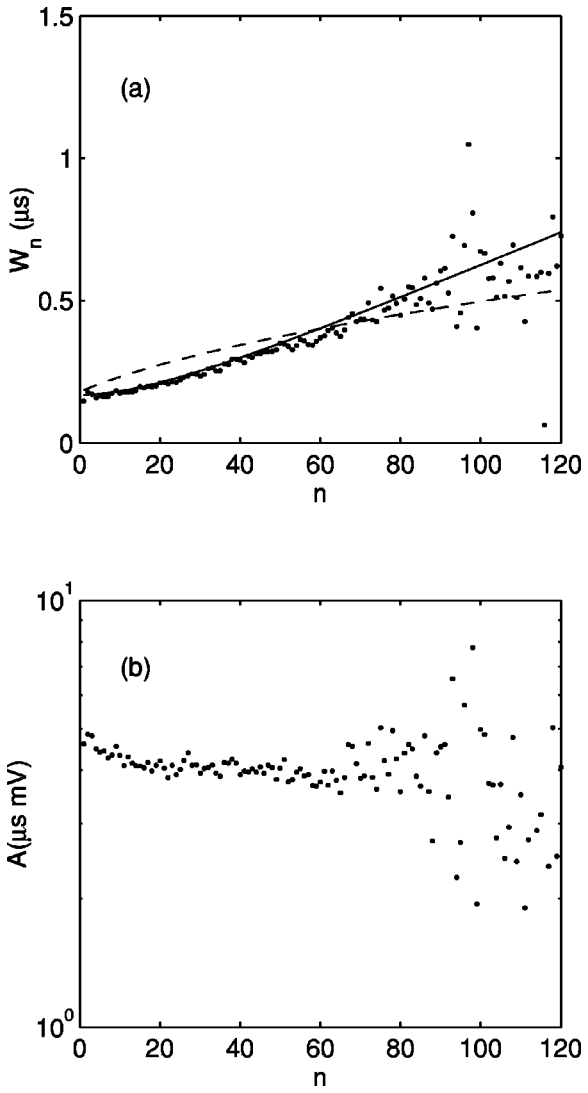


FIG. 4. Evolution of a bunch of 4.2 keV $Ar^+$ with initial width of ~170 ns when $V_1 = 5.5$ kV as a function of the number of oscillations *n*. (a) The measured bunch width $W_n$ (dots). The solid line shows a fit to the data with Eq. (10), where $W_0 = 167$ ns and $\Delta T_p = 5.9$ ns. The dashed line shows a fit to the data with Eq. (11), where $W_0 = 167$ ns and $\Delta T_p = 46.3$ ns. (b) The area *A* under the pulse.

where *A* is the area under the peak, $W_n$ the bunch width, $t_b$ the average time of arrival of the bunch at the center of the pickup, and *a* and *b* the coefficients of the linear background. The values of *A*, $W_n$, $t_b$, *a*, and *b* were free parameters for each peak. The dots in Fig. 4(a) show the bunch width $W_n$ as a function of the number of oscillations *n*. As the period of oscillation is 3.15 $\mu$s, 100 oscillations represent about 315 $\mu$s of storage time. The initially confined bunch of ions is seen to broaden with a characteristic dependence on the number of oscillations. Although $W_n$ increases significantly with time, it is shown in Fig. 4(b) that the peak area, which is proportional to the number of ions in the bunch [see Eq. (3)] decreases only slightly until the bunch is too wide to be measured. Measurements of the lifetime using the MCP detector located outside the trap (see Fig. 1) show that very

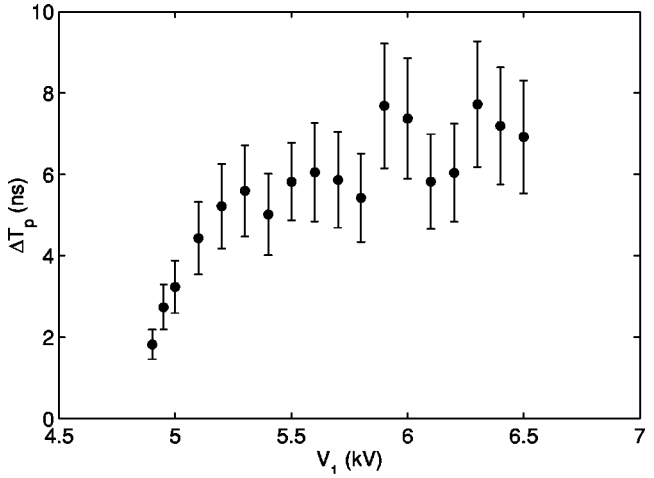


FIG. 5. Measured effective time spread ($\Delta T_p$) as a function of the configuration ($V_1$) of the trap.

few ions are lost from the trap during this time, as a lifetime of about 3 s was observed, corresponding to about $10^6$ oscillations.

The solid line in Fig. 4(a) shows a fit to the width of the bunch using Eq. (10) with $W_0$ and $\Delta T_p$ as fitting parameters. The fit is excellent with $W_0 = 167$ ns and $\Delta T_p = 5.9$ ns. The dashed line in Fig. 4(a) shows the best fit to the experimental data using the expression for noncoherent diffusion [Eq. (11)] with $W_0 = 167$ ns and $\Delta T_p = 46.3$ ns. Noncoherent diffusion is clearly not a good representation of the observed diffusion pattern.

The diffusive behavior illustrated in Fig. 4 is typical for the evolution of bunches for a variety of potential configurations of the trap [14]. In general, with the configurations investigated in this paper, this behavior was seen for $V_1 > 4.9$ kV. Figure 5 shows the fitted values of $\Delta T_p$ according to Eq. (10) for configurations of the trap with $4.9 < V_1 < 6.5$ kV. The value of $\Delta T_p$ rises smoothly from about 2 ns at 4.9 kV to a plateau of about 7 ns for $V_1$ above 6.0 kV.

### B. Synchronization

#### *1. Injection of short bunches*

Up to now, the bunch was shown to evolve smoothly, as would be expected from the statistical assumptions described in Sec. III. In this part, we show that a very different behavior can be obtained for specific configurations of the ion trap.

Figure 6 shows the evolution of an ion bunch injected into the trap with an initial width $W_0 = 130$ ns. In this case, the potential of the first electrode was set to $V_1 = 4.7$ kV. In contrast to the diffusive behavior seen in Fig. 2, the width of this bunch is preserved over the 90 ms shown. More details of the evolution of the bunch are shown in Fig. 7 where the bunch width and peak area are shown as a function of the number of oscillations. The inset in Fig. 7(a) shows the evolution of the bunch width for the first 600 oscillations. During the first 150 oscillations, the bunch width increases much like that for the previous configurations [see Fig. 4(a)], and the solid line shows the behavior according to coherent diffusion [Eq. (10)]. The initial increase in bunch width is accompanied by a decrease in the peak area [see inset in Fig. 7(b)], i.e., ions are lost from the bunch during this stage of the evolution. After the initial increase, the bunch width stabilizes around 120 ns but with some large jumps during the first 5000 oscillations that are correlated with jumps in the peak area. During this time, large amounts of ions are both added to and lost from the bunch. Beyond about 5000 oscillations, the width is essentially constant, although the number of ions in the bunch decreases exponentially with time,

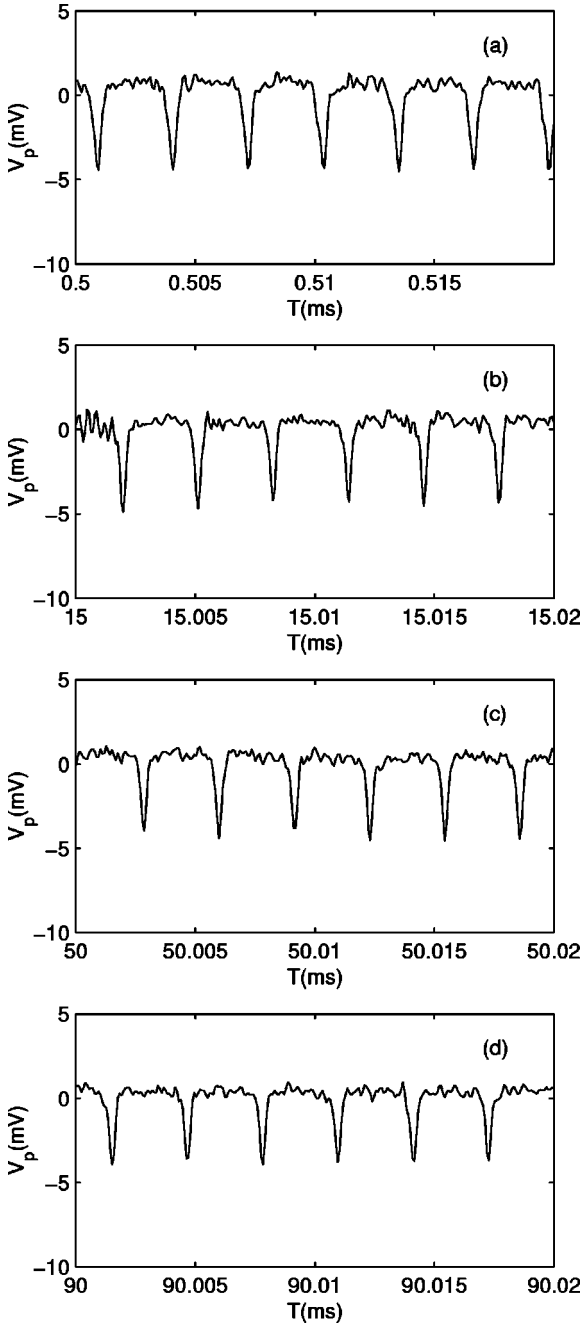


FIG. 6. Signal observed with the pickup for an initially 170 ns wide bunch of 4.2 keV $Ar^+$ stored with $V_1 = 4.7$ kV at four different time intervals after injection: (a) 0.5–0.52 ms, (b) 15–15.02 ms, (c) 50–50.02 ms, and (d) 90.0–90.02 ms.

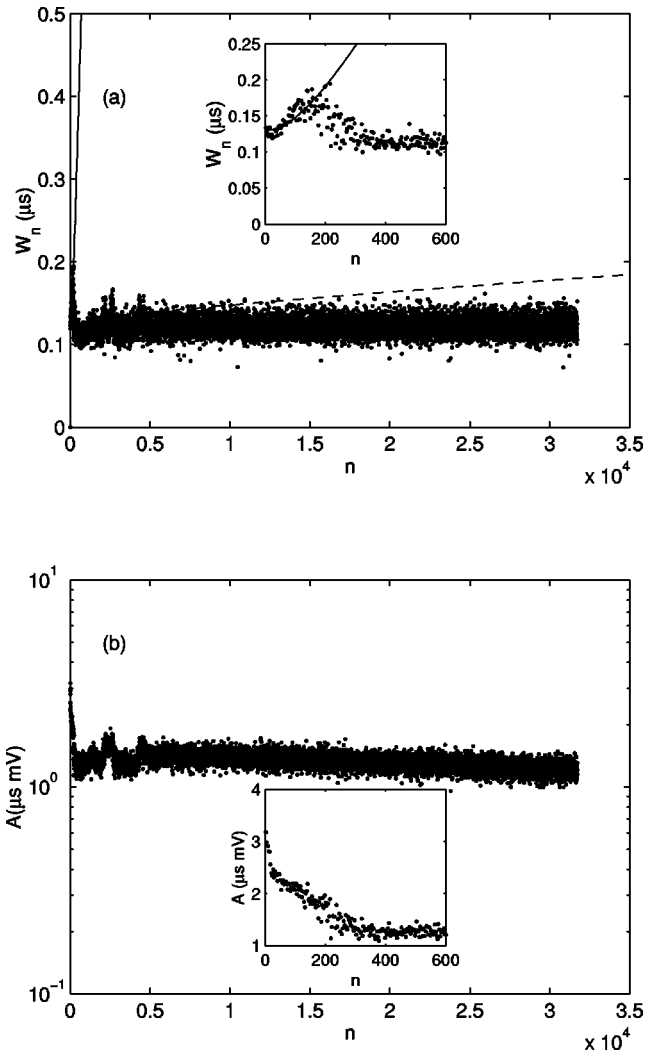


FIG. 7. Evolution of an initially 170 ns wide bunch of $Ar^+$ at 4.2 keV ($V_1=4.7$ kV). (a) Bunch width $W_n$. The solid line is the expected behavior for coherent diffusion [Eq. (10)] and the dashed line is for noncoherent diffusion [Eq. (11)]. (b) The peak area *A*.

with a typical lifetime of 270 ms ($\sim 9\times 10^4$ oscillations). Similar behavior was observed for bunches of initial width $\sim$170 ns injected into the trap for configurations of $V_1 = 4.1$–$4.9$ kV, while above 4.9 kV the initial bunch diffused as described in the previous section (see Figs. 2 and 4). No trapping was achieved for $V_1 < 4.1$ kV. Stable bunches have been observed for up to 330 ms, which corresponds to the maximum memory available for our digital oscilloscope, and, since no change in the asymptotic bunch width was observed on that time scale, one can safely assume that much longer times are possible.

Also plotted in Fig. 7(a) are the expected diffusion patterns for coherent diffusion [Eq. (10), solid line] and noncoherent diffusion [Eq. (11), dashed line]. The evolution of the bunch width as shown in Fig. 7(a) is clearly incompatible with either model, or any intermediate form [Eq. (12)], all of which imply a smooth increase in width with number of oscillations. Thus, the evolution of the bunch cannot be explained by interactions that are stochastic in nature, such as residual gas collisions or noise on the mirror electrodes in the trap. It will be shown that the origin of the nondiffusive behavior illustrated in Fig. 7 lies in the synchronization of the ions' motion that occurs for a range of electrostatic potential profiles in the mirror regions.

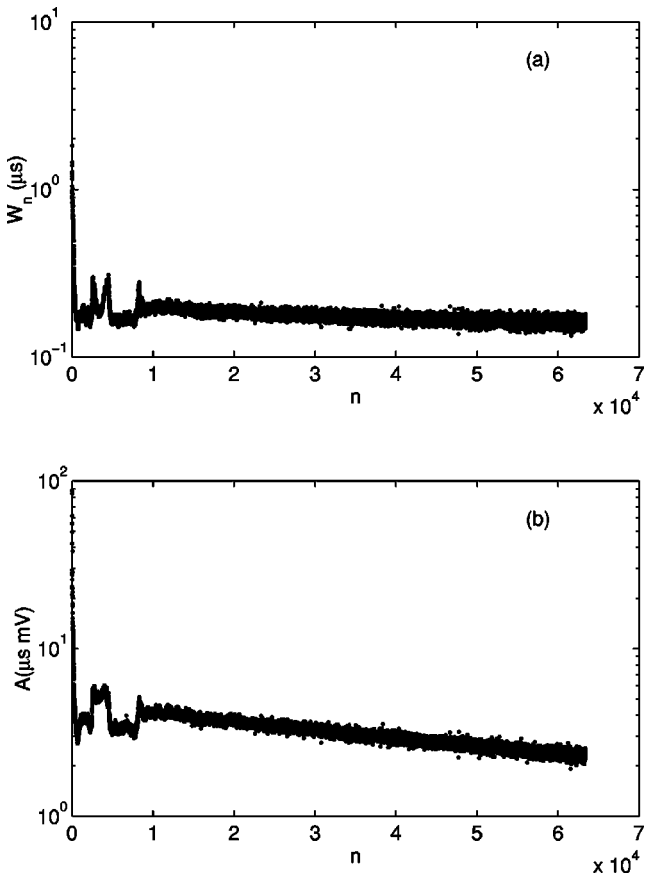


FIG. 8. Evolution of a bunch for an initially 0.9 $\mu$s wide bunch of $Ar^+$ at 4.2 keV ($V_1=4.7$ kV). (a) Bunch width $W_n$ as a function of the number of oscillations. (b) Peak area *A* as a function of the number of oscillations.

### *2. Asymptotic behavior*

The synchronization phenomenon was investigated by studying the bunch development for different configurations of the electrode potential $V_1$, initial bunch widths, and different ions, namely, $Ar^+$ and $Xe^+$. When a wide bunch of ions was injected into the trap it was observed to split up into narrower bunches during the first tens of milliseconds, while only one narrow bunch with a characteristic width remained at later times. Figure 8 displays the details of this evolution for an initially 0.9 $\mu$s wide bunch of $Ar^+$ at 4.2 keV when the trap was configured with $V_1=4.7$ kV by showing the fitted width [Figs. 8(a)] and area [Figs. 8(b)] [see Eq. (13)] of the largest bunch as a function of the number of oscillations. After a rapid shrinking of both the bunch width and pulse area (which correspond to a loss of particles from the bunch) during the first 500 oscillations, the largest ion bunch captures and releases other bunches for about 8000 oscillations.

After about 8000 oscillations, the largest bunch captures the last bunch, leaving in the trap a single bunch of constant

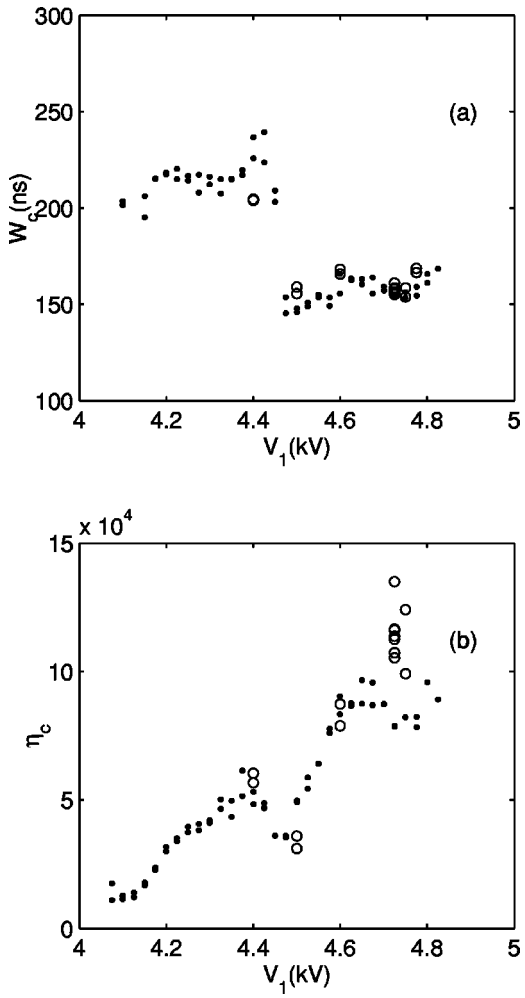


FIG. 9. (a) Asymptotic bunch width $W_c$ for $Ar^+$ (dots) and $Xe^+$ (open circles). For comparison, the data for $Xe^+$ have been multiplied by $\sqrt{40/132}$. (b) Characteristic decay number $\eta_c$ for $Ar^+$ (dots) and $Xe^+$ (open circles). The initial bunch was $\sim 2$ $\mu$s.

width $W_c = 150$ ns, a value close to that measured in the previous case [see Fig. 7(a)]. After this stabilization has occurred the bunch area decreases exponentially with increasing number of oscillations:

$$A(n) = A_0 \exp(-n/\eta_c) \tag{14}$$

where $A_0$ is a constant and $\eta_c$ is a characteristic decay number. For the case shown in Fig. 8(b), $\eta_c = 9 \times 10^4$, corresponding to a lifetime of about 270 ms.

The behavior described above is interpreted as a self-organizing phenomenon, where the route to the organized structure is complex and depends strongly on injection conditions, such as position and angle relative to the trap axis and the initial bunch length. However, once formed, the evolution of the bunch, i.e., its asymptotic width ($W_c$) and decay number ($\eta_c$), depends only the voltage configuration. Similar self-organizing structures were seen for configurations of the trap where the potential of the last electrode was changed in the range $4.1 < V_1 < 4.9$ kV.

The results are summarized in Figs. 9(a) and 9(b) where the asymptotic bunch width $W_c$ and decay number $\eta_c$ are shown, respectively, for a 4.2 keV $Ar^+$ beam (dots), as a function of $V_1$, in the range where synchronization was observed. Each point in the figure represents a separate injection. Two modes are clearly observed, for both the width and the decay number. For values of $V_1 < 4.45$ kV, $W_c$ and $\eta_c$ increase smoothly. At $V_1 = 4.45$ kV, a fast decrease of the asymptotic width occurs, from 240 ns to 150 ns, while $\eta_c$ increases more rapidly from $\sim 5 \times 10^4$ to $\sim 10^5$ oscillations (which corresponds to a bunch lifetime of about 300 ms).

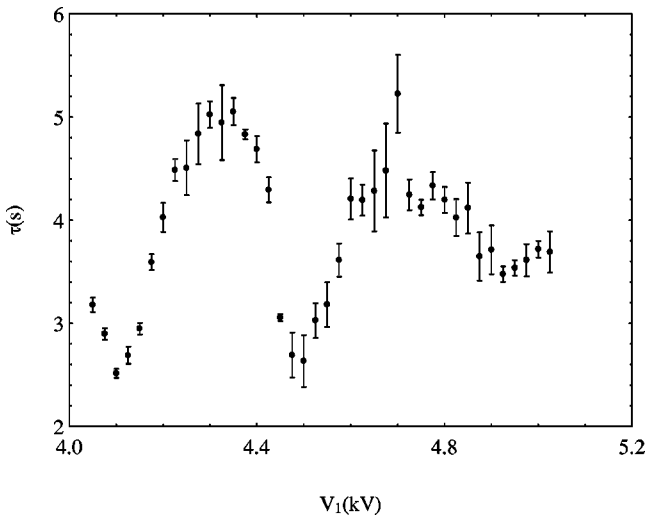


FIG. 10. Asymptotic beam lifetime $\tau$ as a function of $V_1$ for trapped beams of $Ar^+$ at 4.2 kV.

At the same time that the bunch behavior was monitored by the pickup, the overall lifetime of the stored ions was monitored via the MCP. Two decay curves of trapped $Ar^+$ at 4.2 keV are shown in Fig. 3 for two different trap configurations $V_1 = 4.7$ kV and $V_1 = 4.5$ kV, two values for which synchronization is taking place. The decay curves are characterized by strong ion loss within the first $\sim 0.3$ s (i.e., over a time scale corresponding to the bunch lifetime) after which a single exponential decay $\tau$ is observed with a characteristic lifetime of several seconds. Figure 10 shows this asymptotic lifetime of the ion beam as a function of the trap configuration (i.e., $V_1$) over the range where synchronization was observed. In good agreement with the decay number [Fig. 9(b)], $\tau$ also shows two branches where the lifetime varies smoothly, one below $\sim 4.5$ kV and one above.

### *3. Mass dependence*

To further characterize the synchronization phenomenon, Figs. 11(a) and 11(b) show the bunches for 4.2 keV $Ar^+$ and $Xe^+$, respectively, observed 100 ms after injection, using a trap configuration given by $V_1 = 4.7$ kV. The asymptotic width of the bunches is clearly larger for $Xe^+$ than for $Ar^+$. Some measured widths of $Xe^+$ with different trap configurations are plotted as open circles in Fig. 9. For better comparison with the results for $Ar^+$ (dots), the values for $Xe^+$ have been multiplied by the square root of the mass ratio of argon and xenon, which is equal to their velocity ratio. With this scaling the asymptotic widths for $Ar^+$ and $Xe^+$ bunches

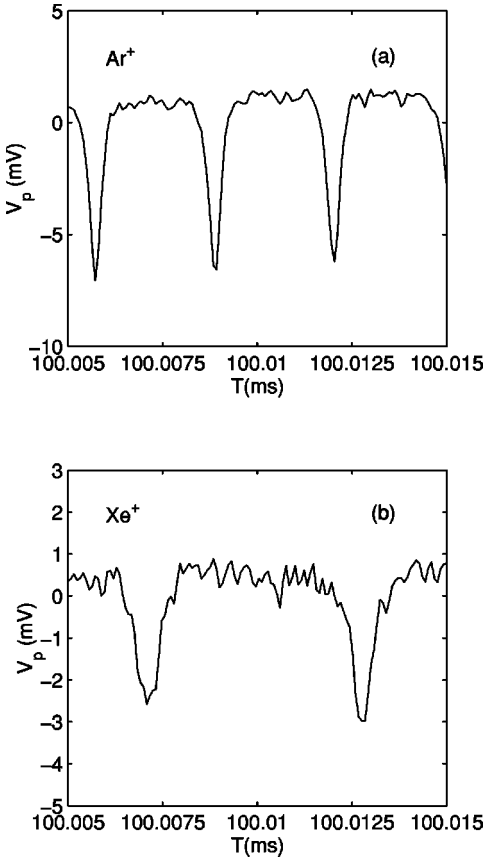


FIG. 11. Asymptotic bunch width $W_c$ 100 ms after injection for (a) $Ar^+$ and (b) $Xe^+$ with $V_1=4.7$ kV. The injected bunch width was about 5 $\mu$s.

agree very well. As the bunch width $W_c$ is given in units of time, this agreement demonstrates that the bunch widths in units of length for both $Ar^+$ and $Xe^+$ are identical. The decay numbers ($\eta_c$) [Fig. 9(b)] are in reasonable agreement for the two species as well.

## V. ONE-DIMENSIONAL MODELS OF SYNCHRONIZATION

In this section we demonstrate that the source of the synchronization for ions trapped in an electrostatic potential is the repulsive Coulomb force between them. To illustrate how repulsion can counteract diffusion and to gain further insight into the dynamics of diffusion and synchronization, we have numerically studied two models: The first is based on the mean field approximation, while the second is a multiparticle calculation with interacting ions. In both cases, we assume the system to be trapped in a one-dimensional flat-bottomed potential. Clearly, a one-dimensional model is a rather crude approximation of the experimental situation. However, as will be shown, important characteristics related to diffusion and synchronization can be understood with the insight gained through these models. A detailed analysis of the data will be given in Sec. VI.

### A. The model potential

A drawing of the model potential is shown in Fig. 12, and

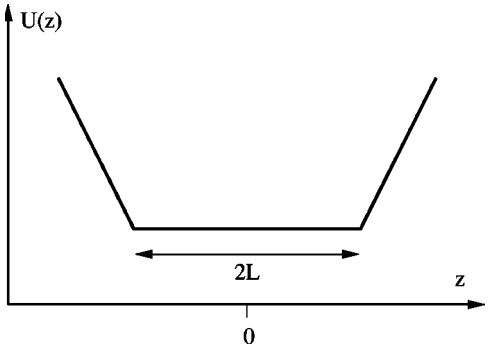


FIG. 12. The one-dimensional model potential used in the simulations. The slope of the potential wall is $\alpha_w$.

the potential is explicitly given by

$$U(z)=\begin{cases} 0 & \text{if } |z|\leq L \\ \alpha_w(|z|-L) & \text{if } |z|>L, \end{cases} \tag{15}$$

where $2L=200$ mm is the length of the field-free region and $\alpha_w$ is the slope of the potential walls. It is important to realize that in such a potential the period of oscillation is not a monotonic function of the particle kinetic energy: For an $\alpha_w<2E/(qL)$, the oscillation period of fast particles is longer than for slow particles. This is because the fast particles climb higher on the potential wall, and the extra time spent in this region is larger than the time difference between slow and fast particles in the field-free region. There is a slope $\alpha_w=2E/(qL)$ for which the period of oscillation $T$ of the particles is independent of small variations of their kinetic energies $E$. Under such a condition ($dT/dE=0$) the diffusion of a bunch of particles moving in this potential is strongly reduced. A convenient parameter to characterize the motion of a single ion in this potential is the logarithmic derivative $\alpha$ of the oscillation time $T$ with respect to the ion energy $E$:

$$\alpha=\frac{1}{T}\frac{dT}{dE}. \tag{16}$$

This parameter is directly related to the slope of the potential walls by

$$\alpha=\frac{1}{2E}\frac{1-L(q/E)(\alpha_w/2)}{1+L(q/E)(\alpha_w/2)}. \tag{17}$$

While the slope of the potential wall is bounded by $\infty>\alpha_w>0$, $\alpha$ takes values in the interval $-1\leq\alpha\times 2E\leq 1$. All properties of the single ion motion can be expressed through $\alpha$. Here we are particularly interested in the oscillation time, which is given by

$$T(\alpha)=\sqrt{\frac{M}{2E}}\frac{4L}{1-2E\alpha} \tag{18}$$

where $M$ is the ion mass.

Another important feature of the one-dimensional potential model is that for a given value of $\alpha$ and a specific $M$ a small change in the energy is directly related to a change in oscillation time $\Delta T$ by

$$\Delta T = \Delta E \left| \frac{dT}{dE} \right| = \Delta E |\alpha| T(\alpha). \tag{19}$$

### B. Mean field approximation

In this model, we consider the motion of a test ion of mass $M = 40$ amu and charge $q = |e|$ and a sphere of radius $R$ uniformly filled with $N$ identical ions moving together in the potential given by Eq. (15).

The main goal here is to understand the behavior of a single ion in the field created by all other ions, which are represented by the charged sphere. The force between the ion and the sphere is given by

$$F_m(\Delta z) = \frac{e^2}{4\pi\varepsilon_0} \frac{N}{R^2} \times \begin{cases} \dfrac{\Delta z}{R} & \text{if } |\Delta z| \leqslant R \\ \dfrac{R^2}{\Delta z^2} & \text{if } |\Delta z| > R \end{cases} \tag{20}$$

where $\Delta z$ is the separation between the test ion and the center of the charged sphere.

In the real three-dimensional potential the ions are compressed radially by focusing and longitudinally by the reduction of velocity inside the electrostatic mirrors. To emulate this behavior, the radius of the sphere was changed as a function of its velocity using the following dependence:

$$R = R_{min} + (R_0 - R_{min}) \frac{v}{v_0} \tag{21}$$

where $R_{min}$ is the minimum possible radius, $R_0$ the radius of the sphere in the field-free region, $v$ the velocity of the sphere, and $v_0$ its initial velocity.

The Newtonian equations for this model system were numerically solved for various values of $\alpha_w$, the initial kinetic energy difference $\Delta E_0$ between the sphere and the test ion, and the charge $N|e|$ on the sphere. The parameters of the sphere were chosen to be $R_0 = 3.6$ mm and $R_{min} = 0.15$ mm for all cases.

Figures 13(a)–13(c) show the value of $\Delta z$ as a function of the number of oscillations for $\alpha \times 2E = 0.5$, $\Delta E_0 = 10$ eV, and different values of $N$. With $N = 1000$ [Fig. 13(a)], the test ion and the sphere separate linearly with time, as expected from the diffusion model. However, for $N = 10\,000$ [Fig. 13(b)], the motions of the test ion and the sphere are highly correlated, and even though the charge on the sphere is larger than in the previous case, the maximum distance between the sphere and the ion is bounded. In short, the motion of the two particles is locked. When the number of ions in the sphere is even larger [Fig. 13(c)], their relative motion becomes more complex, where the test ion and the sphere lock and slip in a complicated pattern, but their separation is still bounded.

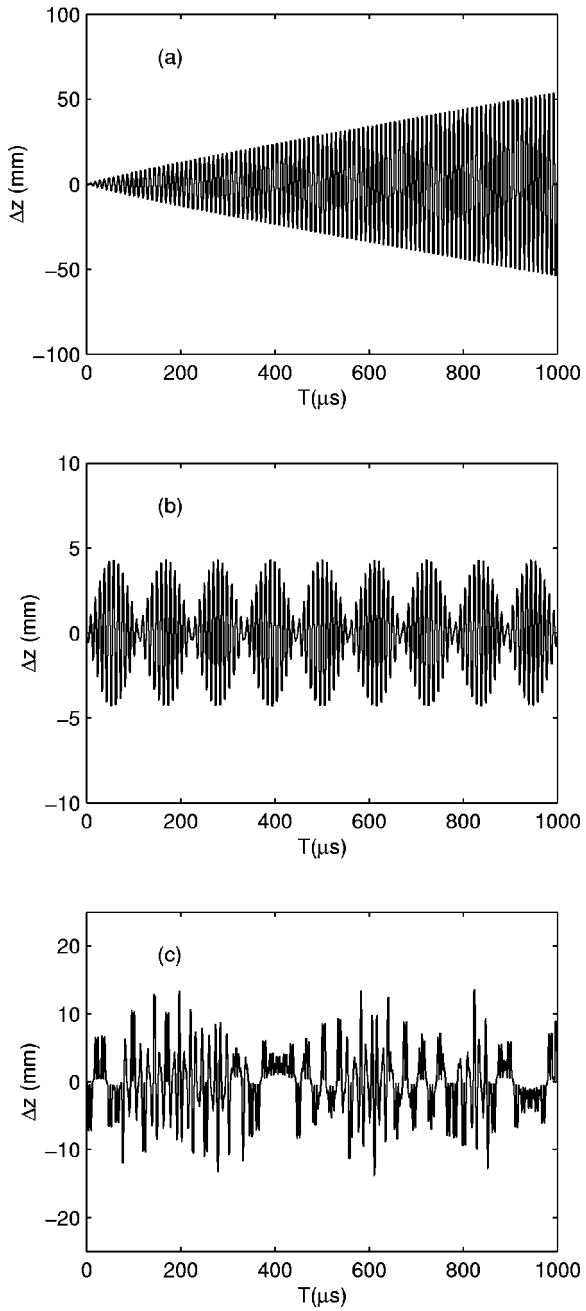


FIG. 13. Three examples of the separation $\Delta z$ of the test ion and the charged sphere as a function of time obtained with $\alpha \times 2E = 0.5$ and $\Delta E_0 = 10$ eV with different numbers of ions in the sphere: (a) $N = 10^3$, (b) $N = 10^4$, and (c) $N = 10^6$.

In order to systematically study the synchronization phenomenon, calculations were performed for various values of $\alpha$ and $N$, for a fixed value of $\Delta E_0 = 10$ eV. In the subsequent analysis, the results were identified as either ''diffusion'' or ''synchronization.'' The result of this analysis is shown in Fig. 14(a). Each point in the figure represents an investigated combination of $N$ and $\alpha$, with open squares indicating a case of ''diffusion'' while filled circles are cases of ''synchronization.'' As pointed out above, the value $\alpha = 0$ is of particular interest as this is where diffusion is strongly suppressed. Figure 14(a) shows that synchronization is ob-

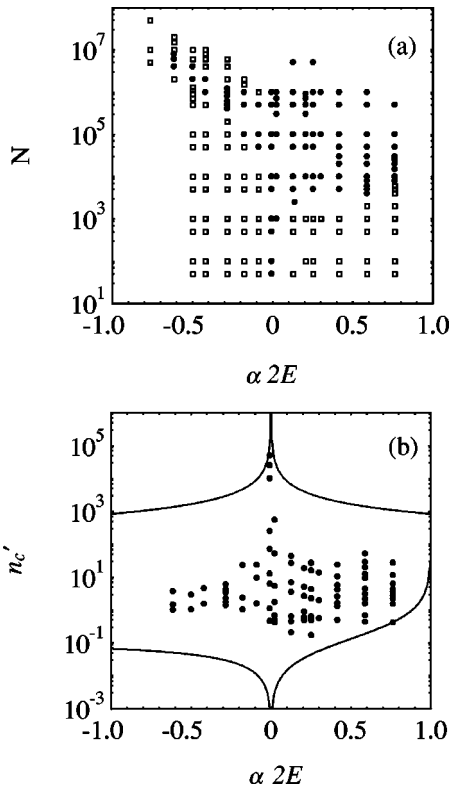


FIG. 14. Synchronization dynamics in the mean field approximation. (a) Number of ions $N$ in the charged sphere vs $\alpha\times 2E$. The open squares represent points where diffusion was observed, and the filled circles represents points where synchronization was found. (b) Comparison between the mean field simulation results and the criterion given in Eq. (38). The plot shows $n_c'=\Delta E_0/\Delta E_c$ versus $\alpha\times 2E$. The test ion had an initial kinetic energy of 4210 eV while the charges in the sphere were initialized with 4200 eV of kinetic energy per ion. The solid circles are the values where synchronization was observed, and the line is given by Eq. (38).

tained not only at this point, but also at values for which $\alpha\neq 0$. In fact, except for $\alpha=0$, there is a minimum and maximum value of $N$ for which synchronization can be obtained. In general, for $\alpha>0$, the range of possible values of $N$ is much larger than for $\alpha<0$, e.g., for $\alpha=0.5$, $2\times 10^3<N<10^6$, while $1\times 10^6<N<2\times 10^6$ at $\alpha=-0.5$.

In summary, the mean field approximation described above illustrates that synchronization can indeed happen among mutually repelling ions bound between two potential walls. Synchronization is strongly favored when $\alpha>0$, and always requires a minimum density of particles to occur.

### C. *N*-body simulations

Another way to illustrate the synchronization phenomenon observed in the electrostatic trap is to study the motion of several interacting ions in the potential given by Eq. (15). The drawback of such a method is the larger CPU time required for completely parametrizing the problem.

Here, we present simulations where a bunch of $N=30$ ions, each of mass $M=40$ amu and charge $q=|e|$, was propagated for 100 oscillations in the potential given by Eq. (15) with different slopes for the potential walls. The width of the bunch was computed as a function of the number of oscillations. For each separate propagation the initial positions of the ions were chosen randomly according to a uniform distribution of mean $\langle z\rangle=0$ and width $\Delta z=0.6$ mm, while their initial kinetic energies were selected randomly from a uniform distribution of mean $\langle E\rangle=4200$ eV and $\Delta E=0.6$ eV. For each value of $\alpha$, one simulation was performed for noninteracting ions and one for ions interacting through the repulsive Coulomb force. In order to allow the ions to overtake each other in this one-dimensional model, the Coulomb interaction was given a minimum impact parameter $\epsilon$ so that the force between a pair of ions $i$ and $j$ separated by a distance $\Delta z_{ij}$ is explicitly

$$F_{ij}=\frac{e^2}{4\pi\varepsilon_0}\frac{1}{\Delta z_{ij}^2+\epsilon^2}. \tag{22}$$

Figures 15(a) and 15(b) illustrate the evolution of this system for $\alpha\times 2E=-0.3$ and $\alpha\times 2E=0.3$, respectively, by showing the calculated bunch width as a function of the number of oscillations. The solid curves show the results obtained with noninteracting ions, while the dots show the results for interacting ions according to Eq. (22) with $\epsilon=1$ $\mu$m. For both values of $\alpha\times 2E$ and for noninteracting ions the ion bunch width increases as expected from coherent diffusion, Eq. (10). For $\alpha\times 2E=-0.3$, the bunch width increases much faster for interacting ions than for noninteracting ions, and in this case the diffusion is enhanced by the Coulomb interaction. In contrast, for $\alpha\times 2E=0.3$ the width of the bunch for interacting ions remains bound between 2 and 4 ns. In this case the repulsion has synchronized the motion of the ions.

The *N*-body simulation also allows us to check the statistical description given by Eqs. (6) and (7). The central quantity that determines the ion dynamics is the correlator $C_n$,

$$C_n=2\langle(T_n-\langle T_n\rangle)(t_{n-1}-\langle t_{n-1}\rangle)\rangle. \tag{23}$$

This quantity holds information in a statistical way on the mechanism of diffusion, as well as synchronization, and measures explicitly the correlation between the arrival times after $n-1$ oscillations and the oscillation times of oscillation $n$. If the value of $C_n$ is positive, the ion bunch will show diffusion, while for a negative value of $C_n$ the ion bunch will tend to synchronize. For instance, the character of the organized state is determined by the requirement $\Delta t_n^2=\Delta t_{n-1}^2$, or equivalently

$$\Delta T_n^2+C_n=0, \tag{24}$$

which is to be evaluated for the synchronized ions, and implicitly requires a negative value of $C_n$. The analysis in Sec. III showed that without ion-ion interaction the correlator will always be positive, $C_n\geqslant 0$. With ion-ion interaction included, the size and sign of the correlator result from the interplay between the ion-ion interaction and the kinematical properties of the electrostatic potential.

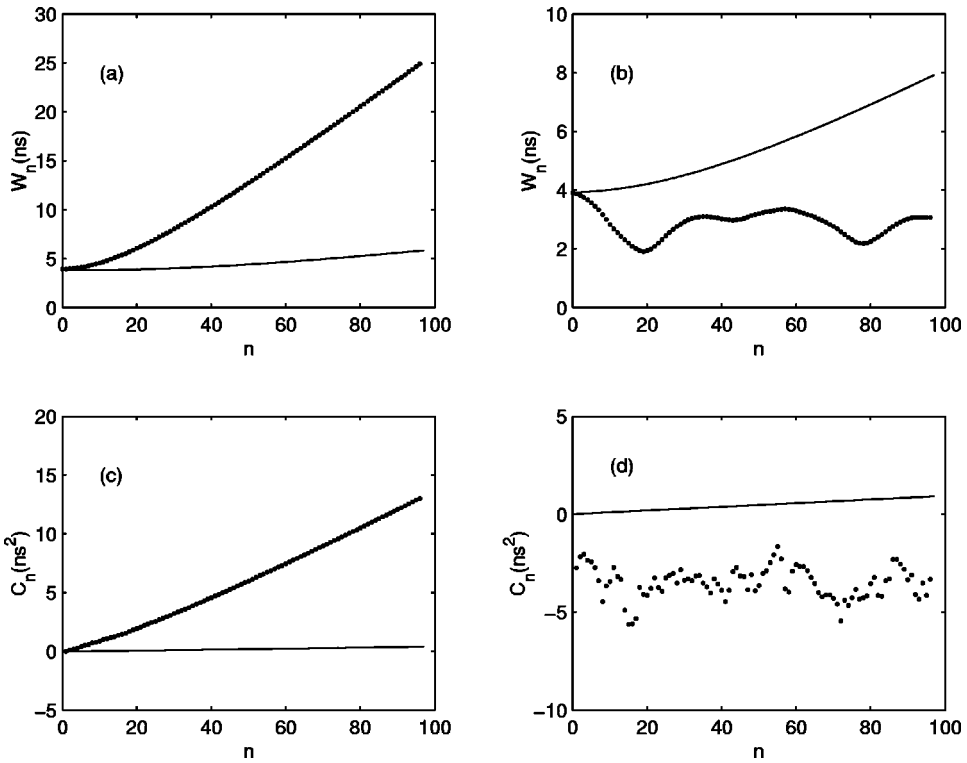


FIG. 15. Evolution of $N=30$ ions, each of mass $M=40$ amu and charge $q=|e|$, trapped in the potential Eq. (15) for two different values of $\alpha$. The initial energies of the ions were randomly selected from a uniform distribution of mean $\langle E\rangle=4200$ eV and width $\Delta E=0.6$ eV. The solid curves show the results obtained with noninteracting ions, while the dots show the results for interacting ions [see Eq. (22)] with $\epsilon=1$ $\mu$m. (a) The width of the ion bunch for $\alpha\times 2E=-0.3$. (b) The width of the ion bunch for $\alpha\times 2E=0.3$. (c) The correlator for $\alpha\times 2E=-0.3$. (d) The correlator for $\alpha\times 2E=0.3$.

Figures 15(c) and 15(d) show the value of $C_n$ for $\alpha\times 2E=-0.3$ (c) and $\alpha\times 2E=0.3$ (d), both for interacting (dots) and for noninteracting (solid curve) ions. While for noninteracting ions $C_n>0$ for all $n$, this is not true for interacting ions when $\alpha\times 2E=0.3$. In this case, the correlator is always negative, and it was found to be negative for all values $0\leqslant\alpha\leqslant 0.9/2E$. Thus, in this case, it is clearly the Coulomb interaction between the particles that is inducing the motion synchronization observed in the simulations.

The dependence of $C_n$ on the number of oscillations can to a good approximation be represented by a linear function [see Figs. 15(c) and 15(d)]. Therefore the evolution of the bunch width can still be well represented by Eq. (10), since here the corresponding correlator equals $C_n=(2n-1)\Delta T_p^2$. Thus, to further quantify the effects of synchronization and enhanced diffusion following from the one-dimensional model, we defined an effective time spread per oscillation $\Delta T_e$ as determined from the linear slope of $C_n$. $\Delta T_e$ was then determined for several values of $\alpha$.

In Fig. 16 $\Delta T_e$ is plotted versus $\alpha\times 2E$. The solid curve shows the behavior expected for noninteracting ions [Eq. (19)], the open circles show the results of the simulation with noninteracting ions, and the solid circles show the results for interacting ions. Where synchronization was observed, the value of $\Delta T_e$ is zero. There is very good agreement between the expected $\Delta T_e$ and that obtained from simulation with noninteracting ions. The small deviation stems from the finite number of ions used in the simulations, which caused the value of $\Delta E_0$ to differ slightly from run to run. For interacting ions, enhanced diffusion, due to the Coulomb repulsion between the ions, is observed whenever $\alpha<0$. At $\alpha=0$ there is a sharp transition to ion motion synchronization, which persists until $\alpha=0.9/2E$, after which the diffusion is much like the diffusion of noninteracting ions. Thus, in the present case, synchronization is observed only for $\alpha>0$. Although a complete parametrization as a function of $N$ was not made (due to the relatively large computational time required for performing these calculations), samples demonstrated that synchronization could also be obtained but only for specific values of $N$ and $\Delta z$ when $\alpha<0$, much as ob-

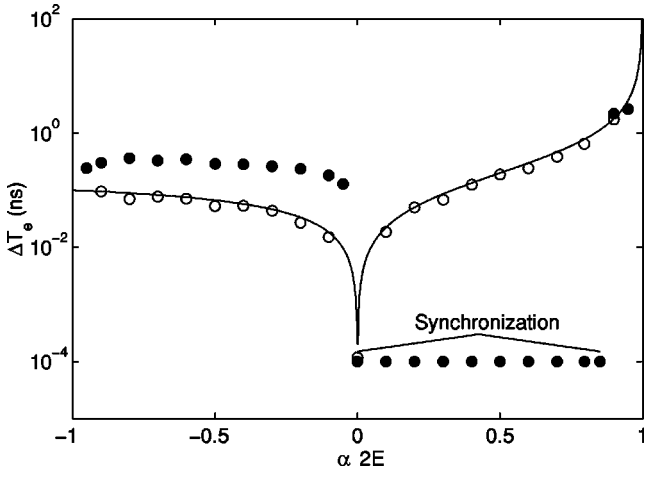


FIG. 16. Effective time spread per oscillation as a function of $\alpha\times 2E$ as obtained from numerical simulations for the same bunches and initial conditions as in Fig. 15. The solid curve shows the expected behavior for noninteracting ions, i.e., $\Delta T_e=\Delta E_0|\alpha|T(\alpha)$. The open circles show the simulation results obtained with noninteracting ions and the dots show the results for ions interacting through the force Eq. (22) with $\epsilon=1$ $\mu$m. The cases for which synchronization occurs, i.e., when $\Delta T_e=0$, are presented on the logarithmic scale by adding $10^{-4}$ ns to their values.

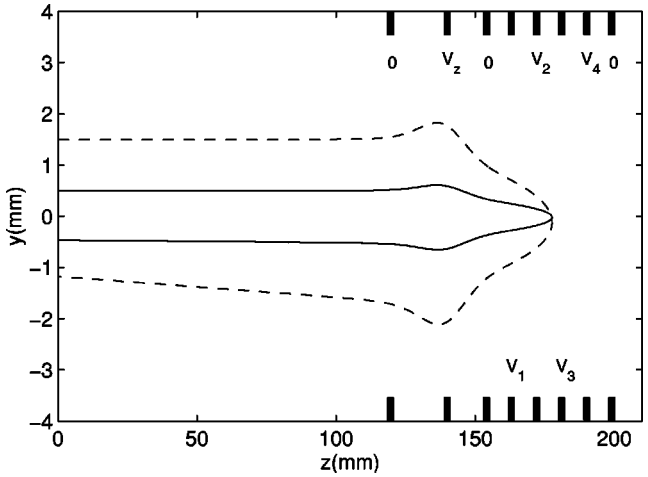


FIG. 17. Two examples of trajectories as calculated with SIMION. The heavy black lines show the location of the mirror electrodes.

served in the mean field model described in the previous section.

In summary, the results of these simulations demonstrate that the Coulomb repulsion between the ions is responsible for the synchronization effect observed in the model potential given in Eq. (15). For synchronization to occur, a minimum density of ions is required, and the effect is greatly favored when $\alpha \geqslant 0$. On the other hand, enhanced diffusion is observed for $\alpha \leqslant 0$. Based on these simulation results, we turn now to a detailed analysis of the experimental data in order to develop general criteria for synchronization and diffusion.

## VI. BUNCH DYNAMICS: DIFFUSION VERSUS SYNCHRONIZATION

In order to gain insight into the diffusion and synchronization as observed in the experiments, numerical trajectory calculations were performed in the actual three-dimensional potential of the trap. We used the SIMION program [17], which can both solve the Laplace equation for a specific potential configuration in space, and propagate ions (without ion-ion interaction) on the computed potential grid. The kinematical properties of the trajectories for an ensemble of ions are obtained using Monte Carlo type calculations where the initial coordinates and velocities of the ions are chosen at random from realistic values. Two examples of ion trajectories can be seen in Fig. 17, where only half of the trap is shown (the value of $V_1$ was set to 4.7 kV). Details about these calculation can be found in Ref. [13].

### A. Diffusion

Using trajectory calculations, it is possible to quantify and interpret the experimental diffusion patterns observed in Fig. 4(a) for $V_1 > 4.9$ kV. As pointed out in Sec. III, when external and internal perturbations are neglected, there are two contributions to the time spread per oscillation, namely, the intrinsic time spread $\Delta T_i$ and the time spread $\Delta T_v$ associated with the initial energy spread.

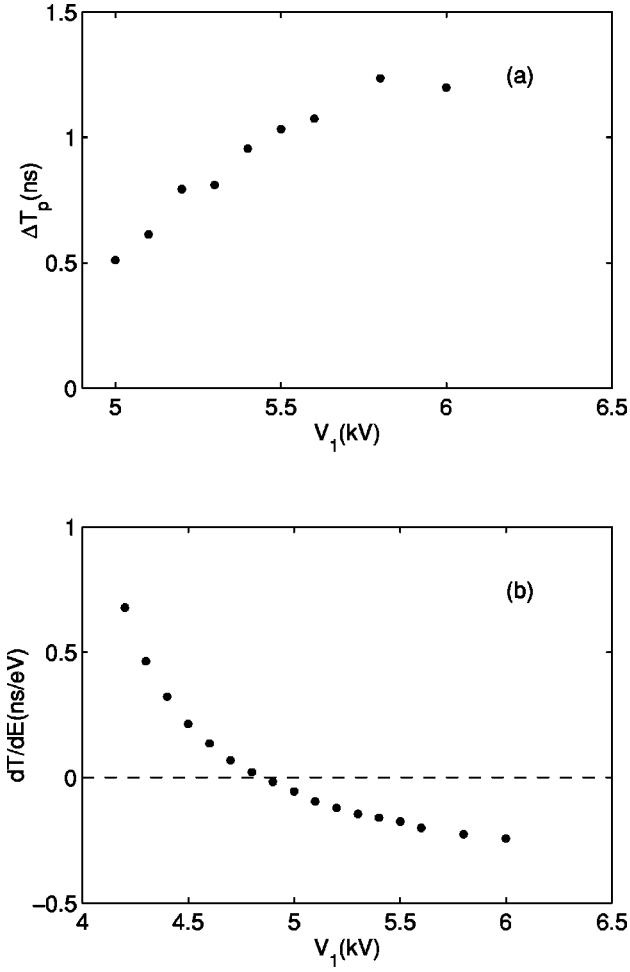


FIG. 18. Calculated parameters of the diffusion as a function of the trap configuration ($V_1$). (a) Total time spread per oscillation, $\Delta T_p$. (b) Mean value of the derivative of oscillation time with respect to energy, $(dT/dE)$, at $E = 4200$ eV.

The intrinsic time spread $\Delta T_i$ was obtained directly from SIMION by filling the trap with a beam with a Gaussian profile of width $\sigma(x) = \sigma(y) = 2$ mm, where $r = \sqrt{x^2 + y^2}$ is the radial coordinate, and a Gaussian distribution of the radial component of velocity $v_r$, of width $\sigma(v_r/v_t) = 0.001$, where $v_t$ is the speed. Analysis of the oscillation times was then performed and the widths (corresponding to $\Delta T_i$) were obtained for different values of $V_1$.

To evaluate $\Delta T_v$, the derivative of the oscillation time with respect to energy, i.e., $dT/dE$, must be calculated for the populated trajectories. This value was also extracted from SIMION calculations, and folded with a realistic value of energy width $\Delta E_0 = 1$ eV, to obtain the time spread $\Delta T_v$.

The total time spread $\Delta T_p = \sqrt{\Delta T_v^2 + \Delta T_i^2}$ was calculated, and the results are shown in Fig. 18(a) as a function of $V_1$. Comparison of these results with the experimental data (Fig. 5), for values where synchronization was not observed, i.e., $V_1 > 4.9$ kV, shows that the calculation underestimates the time spread by a factor of $\sim 4$, although the overall shape is reproduced correctly. The value of $\Delta T_p$ is dominated by the intrinsic time spread $\Delta T_i$, and the dependence of $\Delta T_p$ on $V_1$ as shown in Fig. 18(a) mainly reflects the variations of the

available phase space under the injection conditions used.

The explicit values of $dT/dE$ calculated using SIMION, and which are used to calculate the $\Delta T_v$ contribution, are plotted in Fig. 18(b). It is seen that $dT/dE$ changes sign around 4.9 kV, i.e., $dT/dE<0$ for $V_1>4.9$ kV, which is the region where diffusion is observed in the experiment. This is also fully consistent with the results of the one-dimensional simulations, which showed that diffusion is favored in the region $dT/dE<0$ (see Fig. 16).

The fact that the measured time spread is larger than the calculated one is consistent with the one-dimensional, many particle simulation results, which show that enhanced diffusion due to the ion-ion repulsion is observed for values of $dT/dE<0$. To estimate the importance of the repulsive Coulomb interaction in the diffusion pattern we first consider a mean field approximation for the ion-ion interaction. When an ion bunch enters one of the electrostatic mirrors it is compressed longitudinally due to the deceleration and radially due to the focusing properties of the mirror electrodes. For the trap configurations used in this study where the ions are strongly focused in the mirror region (see Fig. 17), this compression can increase the ion density by 2–3 orders of magnitude at the turning points as compared to the field-free region. The radial extension of the ion bunch at the turning point can be evaluated from the trajectory calculations, and was found to be of the order of 0.5 mm for all investigated configurations of the trap. Similarly, the longitudinal dimension of an ion bunch can be evaluated from the trajectory calculations, and for a bunch width of 200 ns of $Ar^+$ at 4.2 keV this size is also of the order of 0.5 mm in the mirror region. Thus, assuming that the ion bunch contracts to a sphere of radius $R_t=0.5$ mm at the turning point, the space charge potential at the center of this sphere is

$$U_s=\frac{3}{2}\left(\frac{e}{4\pi\epsilon_0}\frac{N}{R_t}\right), \tag{25}$$

where $N$ is the total number of ions at the turning point. With $R_t=0.5$ mm and $N=10^6$, this space charge potential becomes $U_s\sim 4$ V. Hence, the energy transferred to the ions in the bunch can be of the order of 4 eV in one oscillation. For $V_1=5.5$ kV, and with a value of $dT/dE=-0.18$ ns/eV [see Fig. 18(b)] this corresponds to a change in oscillation time of $\Delta T_c=0.7$ ns, which when included in $\Delta T_p$ gives a total time spread per oscillation of 1.3 ns. This value is still much smaller than the measured values (see Fig. 5). Thus, evaluated under the mean field approximation, the addition of the Coulomb interaction between the ions still cannot account for the experimentally observed diffusion pattern for $V_1>4.9$ kV (e.g., $\Delta T=5.9$ ns at $V_1=5.5$ kV).

To understand the origin of the enhanced diffusion observed in the experiment (and in the simulation) we return to the ion motion correlator $C_n$ defined in Eq. (23), and analyze in more detail the interplay between the Coulomb repulsion and the kinematical properties of the electrostatic potential. For enhanced diffusion to occur, the value of $C_n$ must be positive and even larger than without ion-ion interaction. This is exactly what was determined from the $N$-body simulation described in Sec. V C, the result of which was shown in Fig. 15(c), i.e., the values of $C_n$ increase faster with interaction than without. Thus, the electrostatic potential must favor interaction conditions for which the ions can diffuse on a time scale faster than the time scale of the repulsive Coulomb force. In other words, there is a correlation between the motion of the ions in a potential well with $dT/dE<0$, which leads to diffusion that is faster than expected from the geometrical trajectory spread, the velocity spread, and simple Coulomb repulsion. Such a correlation can be understood in terms of the kinematics that exist in the potential well shown in Fig. 12.

In a potential well for which $dT/dE<0$, the fast ions have the shorter oscillation times. Thus, during one oscillation, the fast particles will tend to be located at the front of the bunch, while the slowest ones will be located at the rear (tail), thus producing a correlation between position and velocity. Because of this correlation, the Coulomb repulsion force acting between the particles cannot be assumed to be the result of the average space charge potential as given in Eq. (25). In fact, it can be shown that the particles located in the forward part of the bunch will be pushed even more forward, thus increasing their velocities, while the trailing particles will be pushed further to the rear, thereby decreasing their velocities. This combined effect causes the average distances between the ions to grow more rapidly than in a ''mixed'' bunch, where no correlation between position and velocity exists, and it is the basic reason behind the enhanced diffusion observed in the experiments and simulations. Clearly, a minimum density of ions (or number of collisions) is needed for this effect to occur, but it will be shown in the next section, where the synchronization phenomenon is treated, that this minimum is the same for both enhanced diffusion and synchronization. It is important to point out that with a density of ions in the mirror of $\sim 2\times 10^9$ cm$^{-3}$, the time scale of the Coulomb interaction is about 3 $\mu$s, so that the ions gain their additional velocities in only a very small number of oscillations.

### B. Synchronization

#### *1. Criteria for synchronization*

Although the statistical formulation describing the synchronized state has been given in Eq. (24), a more physical description, as well as specific criteria, are needed. In this section, we propose three criteria that have to be met to achieve synchronization.

The first criterion is related to the value of $dT/dE$, i.e.,

$$\frac{dT}{dE}\geqslant 0 \quad \text{(kinematical criterion)} \tag{26}$$

for the potential well in which the ions are moving, and will be called the ''kinematical'' criterion. This criterion can be understood in terms of the kinematical correlation that exists between the ions in the potential well shown in Fig. 12 and has been described in the previous section with the discussion of enhanced diffusion.

As seen from both the experimental data and the simulation, synchronization is easier to achieve when $dT/dE\geqslant 0$.

In this case, the fastest ions have the longest oscillation times. For a bunch oscillating in such a potential well, the fastest ions will tend to localize in the rear of the bunch, while the slowest ones will tend to be located at the front. The correlation produced here is thus the inverse of the one for enhanced diffusion (when $dT/dE<0$), and the effect of the Coulomb interaction between the particles is accordingly different: The fast particles, located at the back, will have their velocities reduced by the Coulomb force, while the slow ions, located at the front, will be pushed further ahead, thereby increasing their velocities. The combined effect is to move the rearward particles toward the front of the bunch, and the leading particles toward the back, hence keeping the size of the bunch constant. Thus, the particles will have relative motion of the type shown in Fig. 13(b). For high density of ions, when the Coulomb force can no longer be considered as a perturbation, a more complex pattern will emerge, as observed in Fig. 13(c). Clearly, the kinematical effect is not sufficient, as interaction (collision) between the particles is needed, and this will be taken care of by two additional criteria.

The second criterion is that for a group of trapped ions to show synchronization, they must all be able to collide (interact) with each other. This means that the phase space they occupy must be coupled by collisions. This will be called the ''focusing'' criterion. In the electrostatic trap, the ion-ion collisions are of importance only in the mirror region, where the density is the highest [13]. Thus, the focusing criterion can be established by considering the trajectory properties at the turning points, which are a direct function of the potential configuration on the electrode mirrors, and, more specifically, on the potential close to the turning point itself, i.e., $V_1$. Trajectory simulations performed using SIMION show that the trap configurations used in the present study are all characterized by strong radial focusing of the beam inside the mirror, an effect that originates in the relatively high value of $V_z=4.06$ kV. The trajectories shown in Fig. 17 clearly demonstrate that the ions meet at the turning point, so that strong compression of the bunch occurs, facilitating the collisional coupling of their trajectories. However, due to the cylindrical symmetry of the electrostatic potential of the ion trap, the angular momentum $L_z$ about the symmetry axis is a constant of motion for the individual ions. Consequently, the ions will tend to separate radially at the turning points according to their angular momenta, implying that only ions with similar angular momenta will be able to interact at these points. The criterion that the phase space of synchronized ions must be coupled by collisions implies both strong spatial compression of the ion bunch and similarity of the angular momenta of the ions. This criterion can be stated to a first approximation as

$$\Delta z_t = R_t \quad (\text{similar } L_z) \quad (\text{focusing criterion}) \tag{27}$$

where $\Delta z_t$ and $R_t$ are the axial and radial sizes of the bunch, respectively, at the turning point. Using a second order expansion for the bunch position around the turning point, the axial size at the turning point of an ion bunch of width $W$ can be evaluated as

$$\Delta z_t = \frac{1}{3}\left(\frac{W}{2}\right)^2\left(\frac{q}{M}\right)\left(\frac{dU}{dz}\right)_t \tag{28}$$

where $M$ is the ion mass and $(dU/dz)_t$ is the potential gradient along the trap axis at the turning point. Combining Eqs. (27) and (28), one can extract the asymptotic width $W_c$ of the synchronized bunch, which is given by

$$W_c = k\sqrt{R_t\left(\frac{M}{q}\right)\left(\frac{dU}{dz}\right)_t^{-1}} \tag{29}$$

where $k=350$ ns if $R_t$ is in mm, $M$ in amu, $q$ in units of electron charge, and $(dU/dz)_t$ in V/mm. The value of $R_t$ is peculiar to the trap configuration and the injection conditions, and must be evaluated for the ensemble of ions with similar values of $L_z$. Equation (29) shows that the asymptotic width of a synchronized bunch depends both on the particular type of ion through the mass-to-charge ratio $M/q$ (in agreement with the experimental observation, see Fig. 9) and on the particular configuration of the trap through the potential gradient at the turning points $(dU/dz)_t$ and the radial size of the beam at the turning points $R_t$.

The third criterion states that the collision probability at the turning point must ensure that the ions do indeed lock their motion rather than diffuse and this will be called the ''collision'' criterion. Indeed, as observed in both experiment and simulations, collisions can lead to diffusion or synchronization, even if the kinematical condition is fulfilled, as illustrated in Fig. 16, for $\alpha>0.9$, where it is interesting to note that the diffusion is not enhanced. To quantify this criterion we first note that a group of noninteracting ions will diffuse from an initial width $W$ within a characteristic number of oscillations $n_d$ given by [see Eq. (10)].

$$n_d = \frac{T}{\Delta T_p}\sqrt{1-\left(\frac{W}{T}\right)^2} \tag{30}$$

where $\Delta T_p$ is the width of the distribution of oscillation times [Eq. (8)], which is determined by the initial energy spread as well as the configuration of the trap. As defined, $n_d$ is a lower limit since coherent diffusion has been assumed. As a result of the ion-ion collisions, the oscillation times of the ions are altered. Let us define $\Delta T_c$ as the standard deviation of the distribution of changes in oscillation times upon collision. Then, on average, the number of oscillations $n_c$ that occurs before the oscillation times have been collisionally redistributed among the ions is given by

$$n_c = \frac{\Delta T_p}{\Delta T_c}. \tag{31}$$

For synchronization to dominate over the diffusion due to the initial spread in oscillation time ($\Delta T_p$), the ion-ion interaction must be strong enough that $n_c \ll n_d$. On the other hand, to prevent enhanced diffusion due to the ion-ion collisions, the change in oscillation time due to a collision must also be much smaller than the width of the ion bunch: $\Delta T_c$

$\ll W$. Combining these conditions, the third criterion for synchronization can be expressed as

$$\frac{\Delta T_p}{W} \ll n_c \ll \frac{T}{\Delta T_p}\sqrt{1-\left(\frac{W}{T}\right)^2} \quad \text{collision criterion.} \tag{32}$$

Assuming that the bunch width $W$ is much smaller than the oscillation time $T$, the above criterion has the simple form

$$\frac{\Delta T_p}{W} \ll n_c \ll \frac{T}{\Delta T_p} \quad (W \ll T) \quad \text{collision criterion.} \tag{33}$$

Based on this criterion, the synchronization is seen to be in competition with both the diffusion due to the internal time spread (a property of the trap) and the diffusion due to the ion-ion interaction (and related to the bunch density). In other words, too few collisions or too many lead to diffusion, while there is an intermediate situation where collisions can lead to synchronization. Such a situation can be seen in Fig. 14(a) where for both small and large numbers of ions $N$ in the sphere, diffusion is taking place, while synchronization is the intermediate situation.

#### *2. Numerical estimations*

In this section, we will use the SIMION trajectory calculations to evaluate the quantities needed to compare the synchronization criteria to the experimental values, i.e., the range of potential on the last electrode, $V_1$, for which synchronization was observed.

The kinematical criterion is the easiest to compare. As explained in the previous section, synchronization is strongly favored if $dT/dE \geqslant 0$. Experimentally, synchronization was observed for $4.1 < V_1 < 4.9$ kV, and this range is in very good agreement with the region where $dT/dE \geqslant 0$, as can be seen in Fig. 18(b).

To evaluate the focusing criterion Eq. (27), by use of trajectory simulations we make the simplifying assumption that only ions for which $L_z = 0$ will be able to synchronize through collisions. The radial extension of the ion bunch at the turning point $R_t$ and the gradient of the potential $(dU/dz)_t$ are evaluated using SIMION. Using these values, the asymptotic width $W_c$ is calculated based on Eq. (29). The open circles in Fig. 19 show $W_c$ for configurations of the trap in the range $4.2 \leqslant V_1 \leqslant 4.9$ kV. Two distinct branches of $W_c$ emerge from the trajectory calculations. Below $V_1 \sim 4.45$ kV, $W_c \sim 185$ ns, while for $V_1 > 4.45$ kV, $W_c \sim 165$ ns. The calculated values of $W_c$ are in fair agreement with the experimental values shown in Fig. 9(a), which are also displayed as dots in Fig. 19 for direct comparison. The sudden decrease at 4.45 kV is observed both in the calculation and in the experiment, demonstrating the validity of Eq. (29).

To evaluate the collision criterion for synchronization, Eq. (32), the value of $n_c$ must be estimated. Since $n_c$ is the average number of oscillations before the oscillation times have been redistributed among the ions due to their mutual collisions, it can also be expressed as $n_c = 1/\sqrt{\lambda_c}$ where $\sqrt{\lambda_c}$ is the average number of collisions per oscillation. In a previous publication [13] it was shown that, for a given trajectory $i$, $\lambda_c$ can be estimated as

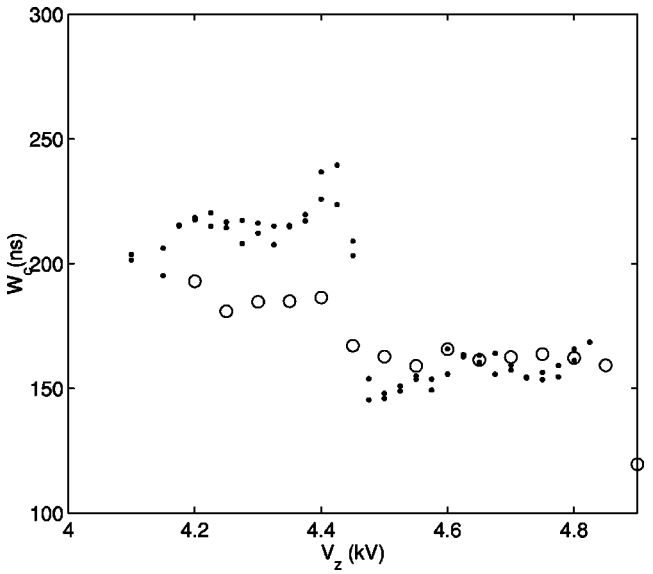


FIG. 19. Calculated asymptotic width $W_c$ as a function of $V_1$ (open circles). The dots are the measured values.

$$(\lambda_c)_i = k'(n_+)_0 \sqrt{\frac{MU_0}{q}}\sigma_{\mathrm{III}}(\Delta v_0)\Delta v_0^2 \times \left(\frac{R_0}{R_t}\right)^2 \left(\frac{dU}{dz}\right)_t^{-1} \left\langle \frac{1}{\Delta v_i} \right\rangle, \tag{34}$$

where $k'$ is a constant, $(n_+)_0$ is the ion density at the center of the trap, $U_0$ is the acceleration voltage, $\sigma_c(\Delta v_0)$ is the ion-ion scattering cross section at a known relative velocity $\Delta v_0$, $(R_0/R_t)$ is the ratio between the beam radii at the center of the trap and at the turning points, $\Delta v_i$ is the relative velocity, and $\langle 1/\Delta v_i \rangle$ is averaged over the relevant phase space at the turning points. For the present configuration of the trap, and the range of values of $V_1$ probed in this experiment, assuming $(n_+)_0 = 10^6$ cm$^{-3}$ and $\sigma_c = 10^{-15}$ cm$^2$, it was found that $n_c \sim 100$. This value can be compared to the limits for $n_c$ as required by the collision criterion in Eq. (32), which are $\Delta T/W \sim 0.01$ (lower limit) and $T/\Delta T = 10^3 - 10^4$ (upper limit). Thus, the value of $n_c$ is well within the required range. An important point here is that, since $n_c$ is related to the density of ions, a wide range of values are possible, and, in particular, bunches of intensities weaker by four orders of magnitude are needed in order to observe a transition from synchronization to diffusion. Unfortunately, such weak beams are undetectable by the present pickup electrode. Also, bunches 10–100 times denser than used in the present experiment are needed to reach the upper limit of synchronization, intensities that cannot be produced by our ion source. Thus, the collision criterion is always satisfied in the present experiment.

An additional check of the collision criterion, Eq. (33), can be made by comparing it with the results of the one-

dimensional mean field simulations (Sec. V B). Consider a bunch of ions oscillating in the potential Eq. (15). The ions have an initial kinetic energy spread of $\Delta E_0$, which is equivalent to a spread in oscillation time according to $\Delta T_0 = \Delta E_0 |dT/dE|$ [Eq. (19)]. For noninteracting ions, diffusion will ensue within a characteristic number of oscillations given by

$$n_d' = \frac{1}{|\alpha| \Delta E_0} \sqrt{1 - \left( \frac{W}{T(\alpha)} \right)^2} \tag{35}$$

[see also Eq. (30)]. The effect of the interaction between the ions is evaluated by first considering the energy transfer $E_c(i,n)$ to an ion $i$ during oscillation number $n$:

$$E_c(i,n) = \int_n F(i) v(i) dt, \tag{36}$$

where the integral is performed over the time of oscillation $n$, $F(i)$ is the summed force from all other ions on the ion $i$, and $v(i)$ is its velocity. The net effect of this interaction is to change the oscillation time of the ion by altering its energy. To evaluate the significance of this effect we consider the standard deviation of the energy transfer $\Delta E_c$. In analogy to Eq. (31) we define a characteristic number $n_c'$,

$$n_c' = \frac{\Delta E_0}{\Delta E_c}, \tag{37}$$

which measures the number of oscillations that occur before the oscillation times (energies) have been collisionally redistributed among the ions.

The criterion for synchronization in the one-dimensional model can then be obtained in a similar way as Eq. (32) by requiring that $n_c' \ll n_d'$ and $n_c' \gg \Delta E_c |dT/dE|$, and becomes explicitly

$$|\alpha| \Delta E_0 \frac{T(\alpha)}{W} \ll n_c' \ll \frac{1}{|\alpha| \Delta E_0} \sqrt{1 - \left( \frac{W}{T(\alpha)} \right)^2}. \tag{38}$$

For bunch widths smaller than the oscillation time, the criterion can be written as

$$|\alpha| \Delta E_0 \frac{T(\alpha)}{W} \ll n_c' \ll \frac{1}{|\alpha| \Delta E_0}. \tag{39}$$

In Fig. 14(b) the results of the numerical simulations are compared to the criterion Eq. (38). The solid circles show the calculated values of $n_c'$ as a function of $\alpha \times 2E$ for the cases where synchronization was observed. The solid lines show the upper and lower limits of $n_c'$ as inferred from Eq. (38). As expected, all points of synchronization lie between the predicted limits. Quantitatively, for synchronization to occur, $n_c'$ must be about an order of magnitude from both the upper and the lower limit.

## VII. DISCUSSION AND CONCLUSION

So far, we have considered that the trapped ions interact directly only through scattering (intrabeam scattering). However, the ions can also interact indirectly through the electromagnetic fields (wake fields) they induce in the surrounding environment. In heavy ion storage rings, intrabeam scattering is known to cause beam loss and increase of the beam emmittance, while the wake field interactions can lead to collective phenomena (coherent instabilities), of which several types have been investigated [18].

The beam interaction is often described by an impedance function $Z$ of the beam environment so that the ions are subject to an additional potential $V = ZI$, where $I$ is the ion current. Evidently, $Z$ is a complicated function, as it must account for all the different structures affecting the beam. At low energy the main source of impedance is the capacitive space charge, while the effect of wall resistivity can be neglected. Further, strong modulations of the ion density can occur due to the wake fields if a structure such as a rf cavity, which has a high $Q$ value and a resonant frequency close to a harmonic of the revolution frequency, exists along the beam path.

The so-called negative mass instability [18], which occurs at relativistic velocities in storage rings, may be the one that most resembles the presently observed synchronization phenomenon. Briefly, the oscillation time of an ion of energy $E$ in a storage ring is given by $T(E) = O(E)/v(E)$ where $O(E)$ is the path length and $v(E)$ is the speed of the ion. Both the path length and the velocity increase with increasing energy, so that an ion with higher energy will travel longer in one revolution, but also faster. At relativistic velocities, where the velocity has only weak energy dependence, $dT/dE$ eventually becomes positive (the energy where $dT/dE = 0$ is called the transition energy). With $dT/dE$ positive, small density perturbations in an initially uniform coasting beam can indeed grow and lead to the formation of several bunches.

The impedance of the electrostatic trap is clearly nontrivial due to the presence of the many closely spaced electrodes along the beam path. In principle, these electrode structures could be resonatorlike and cause collective phenomena to occur. However, the synchronization is seen to occur for ions of different masses for which the oscillation frequencies are very different. Furthermore, the strong dependence of the bunching on the electrode configuration also indicates that resonator type impedances are not driving the synchronization, since in that case the synchronization should be observed for essentially all trap configurations.

From the analysis of collisional properties of the different configurations, the asymptotic width $W_c$ of the bunch is largely reproduced (see Fig. 19). This is a strong indication that synchronization is intimately coupled to direct scattering among the trapped ions. Also, in the numerical simulation, where the wake field interactions are neglected, synchronization emerges, clearly demonstrating that the direct Coulomb force in combination with an electrostatic potential can indeed cause synchronization.

Thus, the phenomenon observed in the present trap appears to be qualitatively different from most of the self-

bunching phenomena known in high energy accelerators [18]. The ion motion synchronization observed in the electrostatic ion trap occurs due to the interplay between the properties of the electrostatic potential and the direct collisions (intrabeam scattering) among the ions, while in storage rings wake fields are the important interaction for coherent instabilities. An interplay between the kinematical properties of the ring and the ion-ion interaction is also a key to understanding the negative mass instability in high energy accelerators.

The ion motion synchronization observed in our trap can also be compared to synchronization phenomena among coupled oscillators [19]. In such a case, each ion can be regarded as an oscillator coupled to the others by their mutual Coulomb interaction. Within this framework, the present ion trap can be characterized as a system of periodic deterministic ocsillators coupled by stochastic interactions, i.e., binary Coulomb collisions. Although the system is in principle deterministic, the large number of oscillators makes the system effectively stochastic [20]. In the present case, the individual oscillators are intrinsically nonstationary as they generally take on slightly different oscillation times in successive turns. Further, the oscillators are only coupled at certain positions in space, i.e., in the mirror regions. Clearly, connections between our observations and the theoretical concepts developed in the field of nonlinear dynamics [19] are needed.

Nonlinear dynamics is well known in several types of ion trap [1], where the most studied cases are the Paul [4] and Penning traps [5]. In particular, collective motion of ion clouds upon excitation with an additional parametrical field has been observed in both of these types of trap [21,22]. In these cases, the origin of the collective motion is an external field, and not the direct scattering among the ions, as in the present case. Also, the effect of Coulomb interactions between trapped clouds of ions of slightly different masses has been studied [23,24].

In this work we have demonstrated the rich dynamics of a packet of ions trapped between two electrostatic mirrors. Experimentally, the evolution of injected ion bunches was observed, and both diffusive and synchronized motion of the ions was seen. These effects have been analyzed with simulations and general arguments related to the kinematical and collisional properties of the system of ions in the trap. We arrived at three criteria that need to be met for synchronization to occur, namely, one related to the kinematical properties, another related to the focusing, and the third related to the collisional properties of the system. Briefly, the kinematical properties of the potential well create a correlation between the velocities of the ions and their positions within the bunch. This correlation, together with the repulsive interaction between the ions, leads to either enhanced diffusion or synchronization of the ion motion.

On the practical side, the synchronization effect described here can lead to several applications. Among them, we have previously proposed the use of such a system for high resolution mass spectrometry [14]. Because the trap is purely electrostatic, the oscillation time of an ion depends on its mass-to-charge ratio as

$$T = \frac{1}{f} \propto \sqrt{\frac{M}{q}}, \tag{40}$$

where $f$ is the oscillation frequency. Hence, by measuring the oscillation time or frequency, the mass-to-charge ratio can be determined. Since, as shown above, it is possible to keep the ions confined in a bunch for a very long time, it might be valuable to try to use such a system for high precision mass spectrometry, much like the so-called Fourier-transform mass spectrometry [25]. In that case, the ions are trapped under the influence of magnetic and electric fields, and undergo cyclotron motion. High resolution is achieved because the ion motion is detected for many cycles, while the packet of ions does not lose its coherence. This is much like the situation we have reached in the present case, when the motion of ions is synchronized. Preliminary results [26] show that indeed very high resolution can be achieved.

## ACKNOWLEDGMENTS

This work was supported by the German Ministry of Education, Science, Research and Technology (BMBF) within the framework of the German-Israeli Project Cooperation in Future-Oriented Topics (DIP), by the Israel Science Foundation, and by the Minerva Foundation.

[1] For a review of ion traps see, e.g., Phys. Scr., T **59** (1995).
[2] D. A. Church, Phys. Rep. **228**, 253 (1993).
[3] L. Schweikhard *et al.*, Phys. Scr., T **59**, 236 (1995).
[4] W. Paul, Rev. Mod. Phys. **62**, 531 (1990).
[5] H. Dehmelt, Rev. Mod. Phys. **62**, 525 (1990).
[6] See, e.g., R. C. Thompson, Adv. At., Mol., Opt. Phys. **31**, 63 (1993).
[7] See, e.g., P. K. Ghosh, *Ion Traps* (Clarendon Press, Oxford, 1995).
[8] D. Zajfman, O. Heber, L. Vejby-Christensen, I. Ben-Itzhak, M. Rappaport, R. Fishman, and M. Dahan, Phys. Rev. A **55**, 1577 (1997).
[9] M. Dahan, R. Fishman, O. Heber, M. Rappaport, N. Altshtein, W. J. van der Zande, and D. Zajfman, Rev. Sci. Instrum. **69**, 76 (1998).
[10] W. H. Benner, Anal. Chem. **69**, 4162 (1997).
[11] A. Fardi, H. Cederquist, and H. T. Schmidt, Hyperfine Interact. **127**, 247 (2000).
[12] H. T. Schmidt, H. Cederquist, J. Jensen, and A. Fardi, Nucl. Instrum. Methods Phys. Res. B **173**, 523 (2001).
[13] H. B. Pedersen, D. Strasser, O. Heber, M. L. Rappaport, and D. Zajfman, Phys. Rev. A **65**, 042703 (2002).
[14] H. B. Pedersen, D. Strasser, S. Ring, O. Heber, M. L. Rappaport, Y. Rudich, I. Sagi, and D. Zajfman, Phys. Rev. Lett. **87**, 055001-1 (2001).
[15] A. L. Rockwood, J. Mass Spectrom. **10**, 241 (1999).

[16] F. Reif, *Fundamentals of Statistical and Thermal Physics* (McGraw-Hill, Singapore, 1985).
[17] Computer code SIMION, Version 6.0, Ion Source Software, Idaho Falls, Idaho.
[18] A. Chao, *Physics of Collective Beam Instabilities* (John Wiley & Sons, New York, 1993).
[19] See, e.g., M. I. Rabinovich, A. B. Ezersky, and P. D. Weidman, *The Dynamics of Patterns* (World Scientific, Singapore, 2000).
[20] H. Sakaguchi, Phys. Rev. E **61**, 7212 (2000).
[21] R. Alheit, X. Z. Chu, M. Hoefer, M. Holzki, and G. Werth, Phys. Rev. A **56**, 4023 (1997), and references therein.
[22] J. Tan and G. Gabrielse, Phys. Rev. Lett. **67**, 3090 (1991).
[23] K. Jungmann, J. Hoffnagle, R. G. DeVoe, and R. G. Brewer, Phys. Rev. A **36**, 3451 (1987).
[24] Y. Naito and M. Inoue, Int. J. Mass Spectrom. Ion Processes **157/158**, 85 (1996), and references therein.
[25] A. G. Marshall and L. Schweikhard, Int. J. Mass Spectrom. Ion Processes **118/119**, 37 (1992).
[26] H. B. Pedersen, B. Amarant, O. Heber, M. L. Rappaport, and D. Zajfman, in *Non-Neutral Plasma Physics: Workshop on Non-Neutral Plasma, San Diego, CA, 2001*, AIP Conf. Proc. No. 606, edited by F. Anderegg, C. F. Driscoll, and L. Schweikhard (AIP, Melville, NY, 2002).